

## Role of Polar Amplification in Long-Term Surface Air Temperature Variations and Modern Arctic Warming

ROMAN V. BEKRYAEV

*Voeikov Main Geophysical Observatory, and St. Petersburg State University, St. Petersburg, Russia*

IGOR V. POLYAKOV AND VLADIMIR A. ALEXEEV

*International Arctic Research Center, University of Alaska Fairbanks, Fairbanks, Alaska*

(Manuscript received 17 June 2009, in final form 1 March 2010)

### ABSTRACT

This study uses an extensive dataset of monthly surface air temperature (SAT) records (including previously unutilized) from high-latitude ( $>60^{\circ}\text{N}$ ) meteorological land stations. Most records have been updated by very recent observations (up to December 2008). Using these data, a high-latitude warming rate of  $1.36^{\circ}\text{C century}^{-1}$  is documented for 1875–2008—the trend is almost 2 times stronger than the Northern Hemisphere trend ( $0.79^{\circ}\text{C century}^{-1}$ ), with an accelerated warming rate in the most recent decade ( $1.35^{\circ}\text{C decade}^{-1}$ ). Stronger warming in high-latitude regions is a manifestation of polar amplification (PA). Changes in SAT suggest two spatial scales of PA—hemispheric and local. A new stable statistical measure of PA linking high-latitude and hemispheric temperature anomalies via a regression relationship is proposed. For 1875–2008, this measure yields PA of  $\sim 1.62$ . Local PA related to the ice–albedo feedback mechanisms is autumnal and coastal, extending several hundred kilometers inland. Heat budget estimates suggest that a recent reduction of arctic ice and anomalously high SATs cannot be explained by ice–albedo feedback mechanisms alone, and the role of large-scale mechanisms of PA of global warming should not be overlooked.

### 1. Introduction

Changes in the arctic climate system over the past decade were exceptional in the history of arctic observations (e.g., Lindsay et al. 2009; Belchansky et al. 2008; Meier et al. 2007; Polyakov et al. 2005; Walsh and Chapman 2001), culminating with the summer of 2007 when the arctic ice retreat broke all records (Stroeve et al. 2008; Comiso et al. 2008). Despite the fundamental importance of high-latitude changes for global climate, there are numerous gaps in our understanding of how the system functions and what forces are driving changes in the Arctic. In particular, information is limited or controversial regarding the role of enhanced high-latitude warming, called polar amplification (PA), in long-term surface air temperature (SAT) variations and modern arctic warming. Positive feedbacks are believed to lead to PA, as shown by analysis of observed SAT (e.g., Vinnikov

et al. 1980; Serreze et al. 2009) and as predicted by general circulation models (e.g., Serreze and Francis 2006; Holland and Bitz 2003). For example, in the ice–albedo feedback mechanism, warming leads to a reduction of ice and snow coverage and decreasing albedo, resulting in further snow and sea ice retreat (Manabe and Stouffer 1980). The most pronounced effect of this feedback, expressed as the strongest ocean–atmosphere upward heat flux and SAT rise, may be found in areas of maximum ice retreat. Recent warm SAT anomalies are consistent with climate model projections in response to reductions in sea ice extent (Overland et al. 2008). Local PA governed by this feedback is seasonal, extending into autumn and early winter, as shown by regional coupled ice–ocean models (Lindsay and Zhang 2005) and global climate models (Murray and Walsh 2005). The exact timing of warming and its magnitude and spatial pattern are, however, sensitive to simulated sea ice retreat, which varies over a wide range from model to model.

There is a host of other important feedbacks leading to PA. Positive feedback related to ice thickness variations is believed to lead to enhanced high-latitude climate change. Model simulations showed stronger PA

Corresponding author address: Igor Polyakov, International Arctic Research Center, University of Alaska Fairbanks, P.O. Box 757335, Fairbanks, AK 99775.  
E-mail: igor@iarc.uaf.edu

with thinner ice cover (Holland and Bitz 2003), confirming earlier modeling results by Rind et al. (1995). This mechanism may be viewed as a part of ice-albedo feedback since thinner ice is subject to faster melt, resulting in more openings in ice cover and a corresponding change of surface albedo (important in summer when there is a lot of sunlight) and heat release from the ocean (important during the cold season). Moreover, heat accumulated by the ocean as a result of the ice-albedo feedback mechanism is partially spent making ice thinner, thus leading in winter and autumn to an increase of SATs (Manabe and Stouffer 1980). Therefore, we will refer to mechanisms related to the change of reflective and insulating properties of the ice/ocean surface as ice-albedo feedback mechanisms. Uncertainties related to modeling both ice thickness and ice extent are substantial (ACIA 2005). Therefore, current model estimates of the quantitative contribution of this feedback to PA should be viewed with caution.

Ice-albedo feedback is widely accepted as one of the strongest mechanisms of PA of global warming (e.g., Manabe and Stouffer 1980). However, Winton (2006) has recently proposed that the ice-albedo feedbacks do not dominate the simulated PA; longwave radiation effects appear to play an equally important role. Using modeling results, Graversen and Wang (2009) suggested even a stronger, dominant, role of the longwave radiation feedback mechanism. Even with the ice-albedo feedback excluded, several GCM studies (Schneider et al. 1997, 1999; Alexeev 2003; Alexeev et al. 2005; Langen and Alexeev 2005, 2007) have found feedbacks involving changes in longwave radiation and turbulent forcing on the high-latitude surface temperature, which are as efficient as ice-albedo feedback mechanisms. These mechanisms of hemispheric-scale PA may be linked to interaction between equator-to-pole air temperature gradients and poleward atmospheric heat transports. These mechanisms will be referred to as the “advection” mechanism of PA. This is a year-round-acting mechanism, amplified during the cold season when the heat and moisture meridional transports are at a maximum. Large-scale PA may also be forced by “local” longwave radiative forcing linking “local to the Arctic” SAT anomalies and changes in surface properties to changes of atmospheric composition (cloudiness and humidity), which has its strongest expression in spring (Francis and Hunter 2007). This will be called the “radiative” mechanism. Note that arctic clouds, particularly in summer, may add strong local arctic flavor to this mechanism (Holland and Bitz 2003). However, the source of high-latitude humidity may still be nonlocal, which could make it difficult to distinguish between local and nonlocal mechanisms.

Experiments with climate models demonstrated that the reduction of the Northern Hemisphere (NH) snow cover may lead to approximately the same increase of radiative heating as that due to reduction of sea ice cover (Winton 2006). Analysis of 1972–2006 satellite observations demonstrated substantial reduction of the NH snow cover, particularly in spring ( $1.26 \times 10^6 \text{ km}^2/35\text{yr}$ , Dery and Brown 2007). The maximum contribution of the positive snow-albedo feedback mechanism should be in spring. We note, however, that the impact of this feedback on PA is not quantified. Moreover, the documented earlier snowmelt by itself may be a result of an increase of incoming longwave radiation due to an increase of SAT and concentration of water vapor in the atmosphere.

Identification of enhanced high-latitude warming using long-term climate trends (i.e., Vinnikov et al. 1980) is complicated by strong arctic intrinsic variability dominated by multidecadal fluctuations (e.g., Polyakov and Johnson 2000; Polyakov et al. 2008). For example, Polyakov et al. (2002) found similar Arctic and Northern Hemispheric air temperature trends during the twentieth century, thus lacking manifestation of enhanced high-latitude warming. However, the exceptional temperature rise observed in the twenty-first century sheds new light on the relative role of PA. We will demonstrate that the ratio of long-term Northern Polar Area (NPA) and NH SAT trends as a measure of PA, widely used in previous studies, may suffer from serious shortcomings. This research assesses enhanced arctic warming via analysis of an extensive collection of meteorological observations including previously unutilized ones and station data that have been updated by very recent (until December 2008) observations. Building upon these measurements, we have evaluated the impacts of PA on large-scale long-term changes of arctic SATs using a new measure of PA.

## 2. Data and methods

The observational database for the NPA consists of monthly surface air temperature (SAT) records from 441 meteorological stations (Fig. 1). Following ACIA (2005), we consider the NPA as the area north of  $60^\circ\text{N}$ . Since interpolation at the southern boundary sometimes requires a wider domain, our collection of data includes observations limited by  $59^\circ\text{N}$ . There are a few exceptions for areas with poor data coverage, where we used observations from the region limited by  $58^\circ\text{--}59^\circ\text{N}$ . In addition, our database includes two very long meteorological records from northern Scotland ( $57^\circ\text{--}58^\circ\text{N}$ ). The only marine meteorological station used in our database is the Weather Ship *Mike*, which provides information from the central Norwegian Sea. Most records have been updated by very recent (until December 2008) observations.

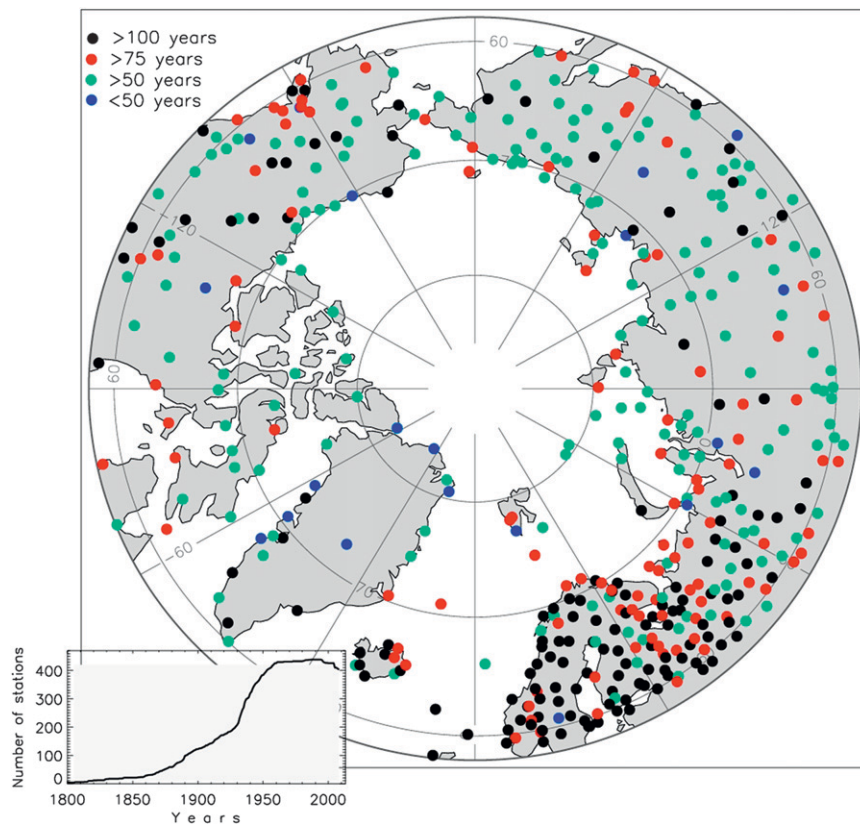


FIG. 1. Map showing locations of meteorological stations. Inset shows the number of active stations for each year since 1800.

The observational database used in this study combines the following datasets:

- monthly mean SATs from the Climate Research Unit, University of East Anglia (CRU UEA) provided by P. Jones;
- monthly data from the Web site of the NOAA National Climatic Data Center (NCDC) and NOAA Global Historical Climatology Network (GHCN), <http://www.ncdc.noaa.gov/oa/climate/ghcn-monthly/index.php>;
- monthly data from the Web site of the Goddard Institute for Space Studies (GISS), <http://data.giss.nasa.gov/gistemp/>;
- monthly data from the University Corporation for Atmospheric Research (UCAR) Web site, <http://dss.ucar.edu/datasets/ds570.0/data/>;
- The Environment Canada, National Climate Data and Information Archive, available online at <http://climate.weatheroffice.ec.gc.ca/climateData/>;
- *The Environmental Working Group Arctic Meteorology and Climate Atlas* (Fetterer and Radionov 2000), available online at [http://nsidc.org/data/docs/noaa/g01938\\_ewg\\_arctic\\_met\\_atlas/](http://nsidc.org/data/docs/noaa/g01938_ewg_arctic_met_atlas/);
- National Snow and Ice Data Center (NSIDC) meteorological data from the Russian Arctic, 1961–2000, available online at [http://nsidc.org/data/docs/noaa/g02141\\_esdimmet/index.html](http://nsidc.org/data/docs/noaa/g02141_esdimmet/index.html);
- monthly SAT for several Russian meteorological stations from the All-Russian Institute of HydroMeteorological Information, World Data Center (RIHMI-WDC) Web site, <http://meteo.ru>;
- monthly and daily data from Alaskan meteorological stations provided by D. Atkinson and M. Shulski;
- hourly data from the NOAA Web site, <ftp://ftp.ncdc.noaa.gov/pub/data/noaa/>;
- daily observations from Russian stations provided by P. Groisman;
- daily data from European stations provided by The Royal Netherlands Meteorological Institute (KNMI) Web site, <http://eca.knmi.nl/dailydata/datadictionaryall.php>;
- hourly data from the Web site of the Russian Academy of Science Space Research Institute, Moscow, Russia, <http://meteo.infospace.ru/>;
- hourly data from the Web site “Raspisanie Pogodi,” <http://rp5.ru>;

- monthly data from the Web site of the Icelandic Meteorological Office, <http://www.vedur.is/>;
- monthly data from the Finnish Meteorological Institute Web site, <http://www.fmi.fi/en/>;
- monthly data from the Web site Rimfrost, <http://rimfrost.no>;
- monthly data from the meteorological station Abisko (Sweden) for 2000–07 provided by C. Jonasson, Abisko Scientific Research Station;
- monthly data from several Scandinavian stations updated using the NordKlim project archive Web site, [http://www.smhi.se/hfa\\_coord/nordklim/](http://www.smhi.se/hfa_coord/nordklim/);
- monthly data for several Scandinavian and Greenland stations updated or corrected using archive created under the Nordic Arctic Research Program project Web site, <http://projects.dnmi.no/~narp/>; and
- data from several Greenland stations from the Danish Meteorological Institute Web site, [http://www.dmi.dk/dmi/tr00-18-data\\_files.zip](http://www.dmi.dk/dmi/tr00-18-data_files.zip).

One of the major previously unutilized and not digitized data sources in our study was the *Climatologic Reference Book of the USSR*, a series published in the 1930s–60s (Rubinshtein et al. 1930, 1933; Climatologic Reference Book of the USSR 1954a,b,c,d, 1956, 1957, 1962). These books contain, among other information, monthly SATs for Russian meteorological stations for separate years from the beginning of instrumental observations. Many stations in the European part of Russia (Russian North) and in West Siberia were established in the middle or end of the nineteenth century. The longest record is from the St. Petersburg station, which was established in 1743. The use of historical Russian archives provided spatiotemporal data coverage for this region of the NPA comparable to that for the Scandinavian region (Fig. 1). Daily and hourly data were processed using data quality control procedure outlined in appendix A.

The record from each station was reduced to monthly anomalies relative to 1961–2000. Annual SAT anomalies were computed only when at least six monthly values were available. These data were used to compose annual and seasonal time series of SAT anomalies for the entire NPA. To minimize the effect of spatially inhomogeneous data coverage, we used a technique similar to the climate anomaly method (CAM) (Jones et al. 1999). In this method, the total area is divided into boxes, and anomaly time series are averaged within each box. The resulting averaged time series for each grid box are averaged again to obtain a single “global” time series. In our case, individual records from land stations over 27 regions were averaged to produce regional time series. Each of the averaging areas was limited by  $10^{\circ}$  along latitude and  $20^{\circ}$  along longitude. The resulting

records were averaged to produce the final record for the entire NPA. Upon comparison, the difference between the two resulting time series (obtained from simple averaging of all available records and by the CAM) is insignificant (for SAT, the correlation is 0.90, and the standard deviations (SDs), which are not statistically distinguishable, are equal to 0.77). Trends in the SAT time series were evaluated by the least squares best-fit method.

Monthly winds, net atmospheric heat fluxes, and ice concentrations were provided by the National Centers for Environmental Prediction (NCEP)–National Center for Atmospheric Research (NCAR) Reanalysis and obtained from the NCAR data server (Kalnay et al. 1996). (These data are used for preparation of Fig. 10 only.) The CRUTEM3v dataset combines SAT over land (Jones and Moberg 2003; Brohan et al. 2006) and is used to obtain NH SAT time series (available online at [www.cru.uea.ac.uk](http://www.cru.uea.ac.uk)).

The major emphasis of this study is an analysis of observations augmented with a model analysis that focuses on the long-term SAT variations. For this purpose, we used 42 available model runs for 1871–1999 from a suite of fully coupled global climate models. These models were used in the Coupled Model Intercomparison Project (CMIP3) (Meehl et al. 2007).

### 3. Northern Polar Area surface air temperatures

Composite annual and seasonal time series of SAT anomalies for the NPA are shown in Fig. 2. NPA temperatures were exceptionally high, reaching  $1.72^{\circ}\text{C}$  in 2003,  $2.11^{\circ}\text{C}$  in 2005, and  $2.18^{\circ}\text{C}$  in 2007, the warmest years in the history of instrumental observations. These years were also associated with the minimum Arctic ice cover. Over the last decade, Arctic warming became stronger and seasonally more uniform compared with warming in the 1930s–40s (Fig. 3). The earlier warming was expressed more in the autumn and winter, with 5–6-yr-long cooling/warming events, whereas since the late 1980s the SAT increase in spring was as strong as in winter and autumn (Figs. 2 and 3). There is, however, substantial spatiotemporal heterogeneity: for example, in winter 2008 SAT in Europe was exceptionally high but a cooler spring and summer made 2008 overall a cooler year compared to 2007 (Fig. 4).

Accelerated warming of the NPA in recent decades is captured by SAT trends (Fig. 2, Table 1). For example, the trend over the last 50 years (1959–2008) was  $0.36^{\circ}\text{C decade}^{-1}$ , increasing to  $0.64^{\circ}\text{C decade}^{-1}$  since 1979. NPA SAT trends over longer periods of time were also very strong, up to  $1.36^{\circ}\text{C century}^{-1}$  for 1875–2008, which is almost two times greater than NH SAT trends ( $0.79^{\circ}\text{C}$

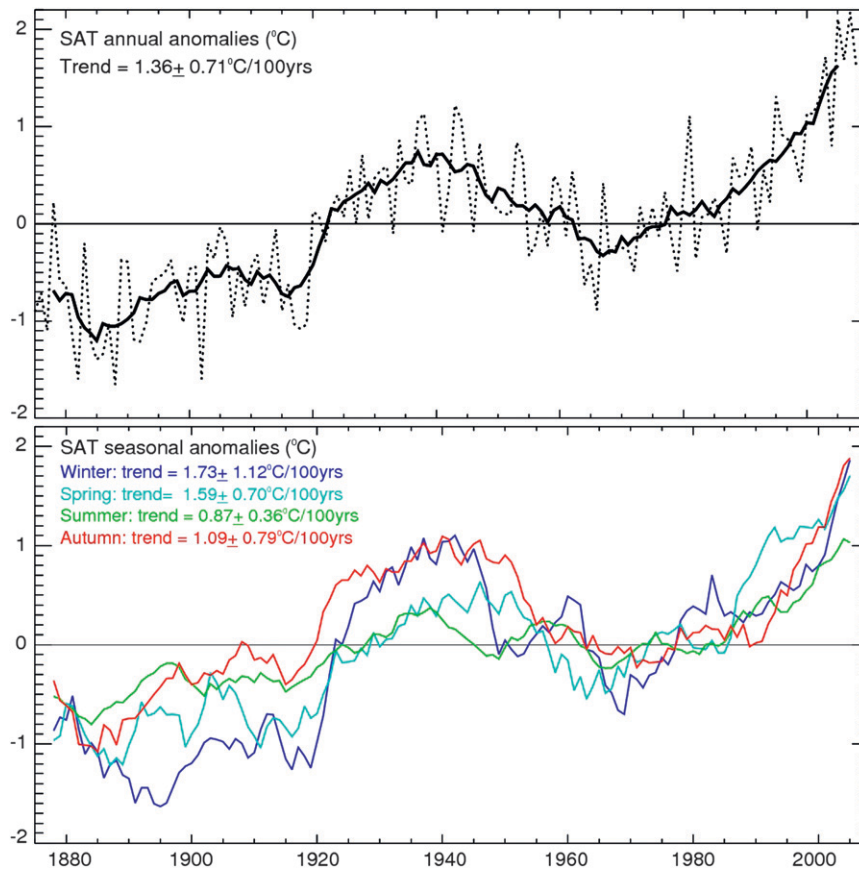


FIG. 2. Composite time series of the (top) annual and (bottom) seasonal surface air temperature (SAT) anomalies ( $^{\circ}$ C) for the region poleward of 59 $^{\circ}$ N. Dotted lines show unsmoothed values; solid lines 7-yr running means. In the legend, trends are for 1900–2008.

century $^{-1}$ ). However, since 1901 NPA trends decreased to 1.20 $^{\circ}$ C century $^{-1}$  (Table 1). Strong multidecadal variability (MDV) affects the behavior of NPA SAT trends, which allowed Polyakov et al. (2002) to suggest that MDV dominates the SAT fluctuations. The inherent difficulty in

differentiating between trends and strong long-term fluctuations makes quantitative analysis of the contribution of trend versus MDV difficult. However, the Arctic warming in the last decade was exceptionally strong, reaching 1.35 $^{\circ}$ C decade $^{-1}$ , thus casting less doubt about

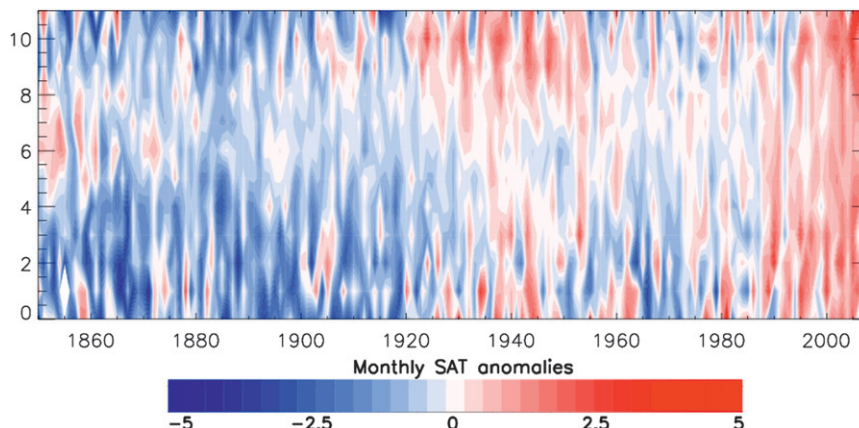


FIG. 3. Year (x axis) vs month (y axis) Arctic SAT anomalies.

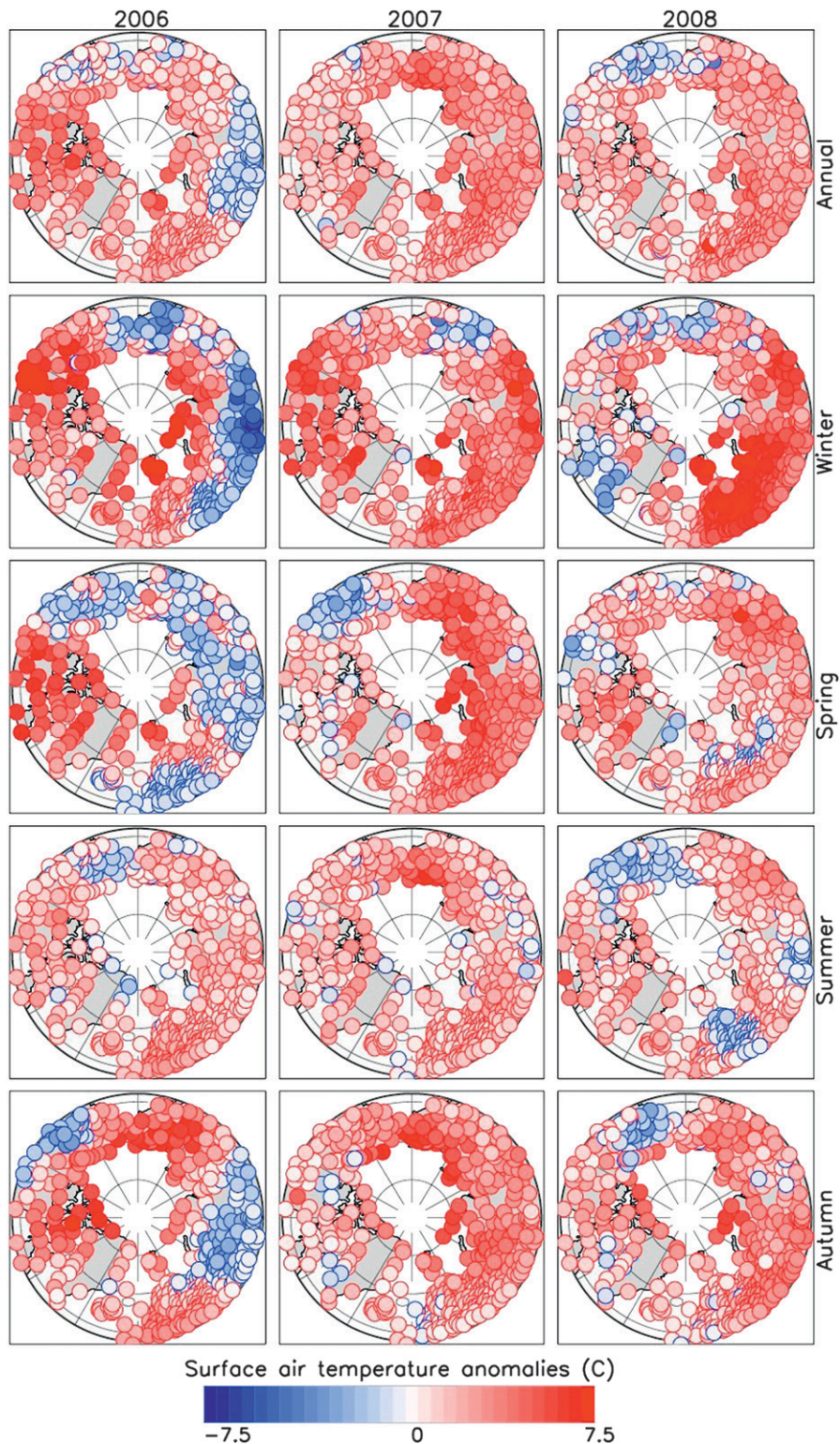


FIG. 4. Annual and seasonal SAT anomalies for 2006–08 from meteorological stations.

TABLE 1. Trends ( $^{\circ}\text{C century}^{-1}$ ) within the Northern Polar Area and for the Northern Hemisphere (*italic* marks trends that are not statistically significant).

	Northern Polar Area					Northern Hemisphere Annual
	Annual	Winter	Spring	Summer	Autumn	
1875–2008	1.36	1.73	1.59	0.87	<i>1.09</i>	0.79
1901–2008	<i>1.20</i>	<i>1.57</i>	1.60	0.88	<i>0.74</i>	0.93
1959–2008	3.64	3.81	4.67	2.34	3.61	2.32
1979–2008	6.39	6.48	7.07	4.37	7.54	3.27

the existence of a long-term externally forced warming trend. Spatial patterns of the SAT trends based on annual data are mostly dominated by positive values (particularly over northern Europe) for both longer (1875–2008 and 1901–2008) and shorter (1979–2008) periods. Negative SAT trends appear for some seasons over limited areas only, mostly in the Pacific sector, probably due to processes governed by the Pacific decadal oscillation. Stronger warming in the maritime region, particularly in autumn and spring (Fig. 5), may be considered as an expression of PA. Understanding the importance of careful evaluation of statistical significance of trends, we propose a new nonparametric approach, which was used in this study (see appendix B for details).

#### 4. Polar amplification

Trends of winter–spring NPA SATs over extended periods of time were generally stronger than in summer–autumn (Fig. 2) and were enhanced compared with the NH trends (Table 1). However, in the recent  $\sim$ 15–20 years, autumnal maritime (<200 km inland) SAT anomalies were amplified (Fig. 5). This change of the seasonal/interannual PA pattern suggests at least two different spatial scales of mechanisms of PA: large-scale (hemispheric) and local (limited by NPA).

##### a. Large-scale PA

A strong contribution of large-scale (hemispheric) PA to the spatial pattern of global warming is evident from, for example, Fig. 6, showing amplification of zonally averaged SAT variations from tropical through high-latitude regions. A similar figure, but for high-latitude ( $>50^{\circ}\text{N}$ ) zonal bands only, was presented by Serreze and Francis (2006, their Fig. 8), who found that the warming in the 1930s was confined to the high-latitude Arctic, whereas the warming that started in the 1970s has more of a “global” expression. Extending the Serreze and Francis Fig. 8 southward (cf. our Fig. 6) provides a new perspective on high-latitude warming. Figure 6 suggests that SATs north of  $55^{\circ}\text{N}$  lead low-latitude SATs, implying the important role of long-term variability in the

North Atlantic forced by high-latitude fluctuations. We note, however, that because of the limited quality of observations and weak signal this suggestion should be viewed with caution.

A direct comparison of Arctic and NH SAT trends used in earlier studies to define a twofold magnitude of the PA (e.g., Vinnikov et al. 1980) may be compromised owing to strong variability, particularly of MDV (Polyakov et al. 2002). For example, the ratio of NPA and NH trends computed for 1924–2000 is  $a_{\text{tr}} = 0.24$ , which is difficult to accept as a measure of accelerated NPA warming. We propose a new quantitative measure of PA linking NPA and NH temperature anomalies  $T'_{\text{NPA}}(t)$  and  $T'_{\text{NH}}(t)$  via a linear regression equation  $T'_{\text{NPA}}(t) = a_r T'_{\text{NH}} + b_r$ . The new measure of PA yields  $a_r = 1.52$  for 1959–2000,  $a_r = 1.62$  for 1875–2008, and  $a_r = 1.45$  for 1901–2008, and these new annual and seasonal regression-based estimates of PA are more stable compared with the estimates based on the ratio of trends  $a_{\text{tr}}$  (Table 2). Particularly striking is the difference between  $a_r$  and  $a_{\text{tr}}$  in autumn, with a vast spread of  $a_{\text{tr}}$  values and a narrow 6% band of  $a_r$  change. Such a drastic difference may be explained by peculiarities of the statistical distribution of  $a_{\text{tr}}$ .

To illustrate this point, we used a suite of 42 CMIP model runs covering the period from 1871 through 1999. Figure 7a shows model-based  $a_r$  and  $a_{\text{tr}}$  with a much stronger spread of  $a_{\text{tr}}$  values compared with  $a_r$  as quantified by a twofold sample estimate of the standard deviation (SD) of  $a_{\text{tr}}$  relative to the SD of  $a_r$ . Dependence of NPA and NH trends with their twofold amplification in the NPA is shown in Fig. 7b. We note that observational and modeling estimates agree well. Some model experiments produce very weak NH trends, resulting in extreme values of  $a_{\text{tr}}$  that have no physical meaning and cannot be used to characterize quality of model simulations. Further analysis of the nature of this phenomenon is possible if we assume that the NPA and NH are statistically independent and that both have normal distributions with zero means. In this case, NPA and NH SAT trends will be subject to a Gaussian statistical distribution with zero means. Their ratio,  $a_{\text{tr}}$ , will be subject to a Cauchy probability distribution, statistical moments of which are not defined (i.e., the so-called heavy tail distribution, Cramer

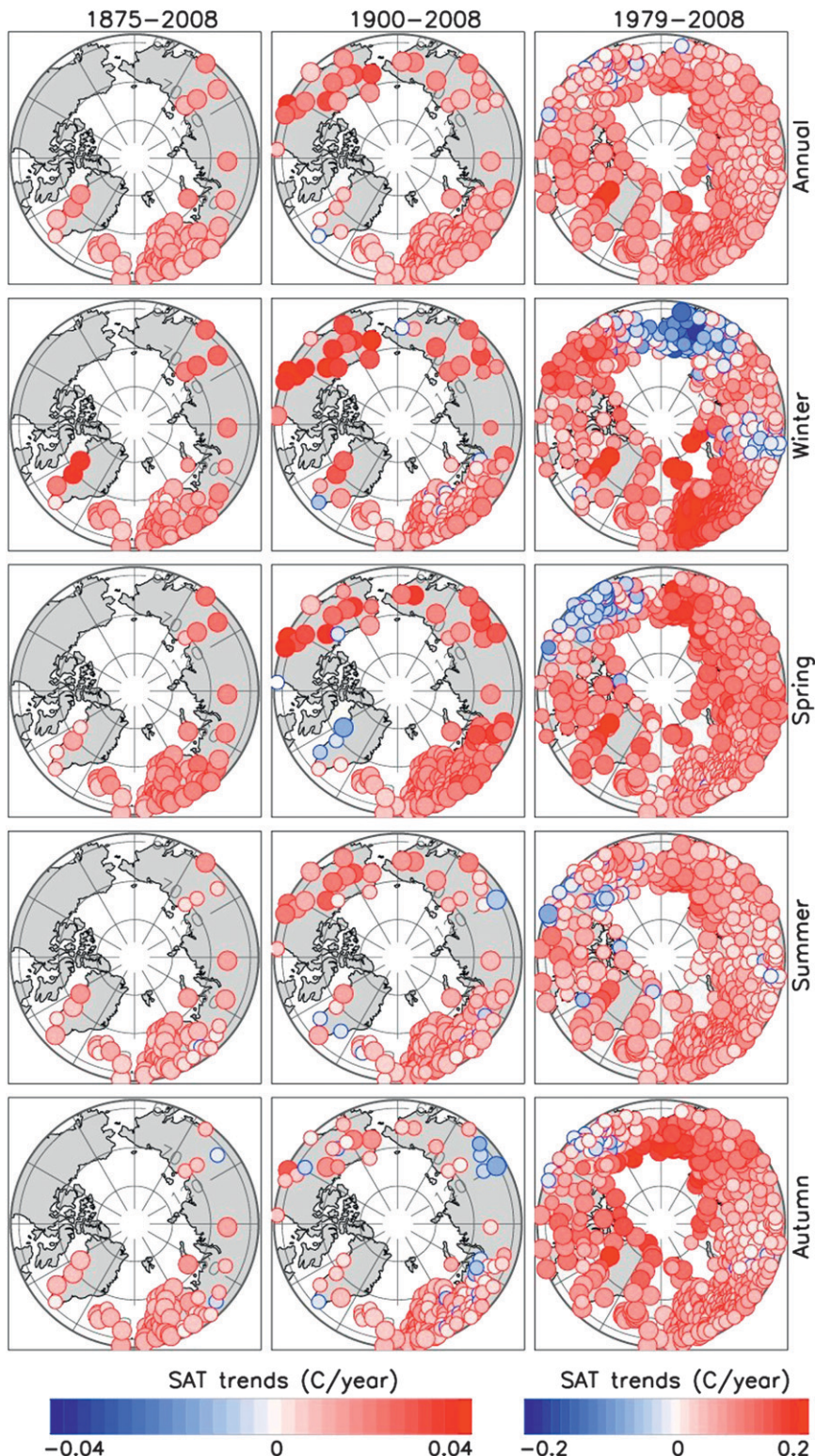


FIG. 5. Maps of annual and seasonal SAT trends based on meteorological station data. Statistically significant trends are marked by larger circles.

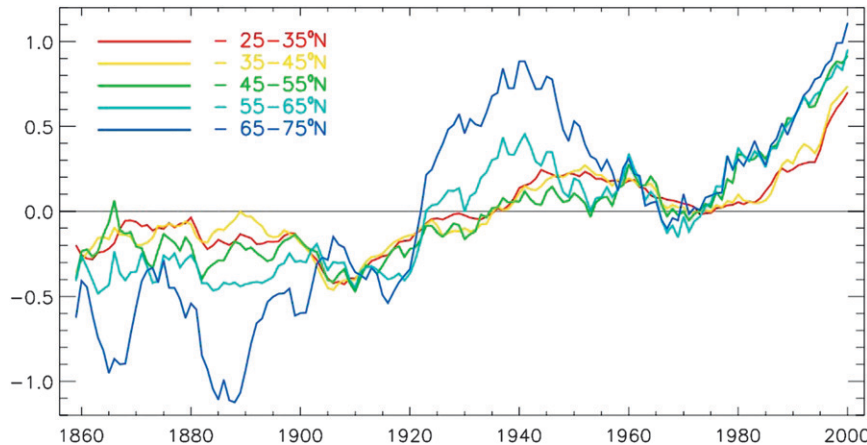


FIG. 6. Seven-year running mean time series of Northern Hemisphere zonal average surface temperature anomalies ( $^{\circ}$ C).

1999). Therefore,  $a_{tr}$  as a measure of PA may lead to unrealistic estimates. Figure 7c shows a time series of SDs derived from an ensemble of model-based  $a_r$  and  $a_{tr}$ . This figure suggests that  $a_r$  provides stable estimates of PA, whereas the wide spread of  $a_{tr}$  precludes the use of  $a_{tr}$  as a meaningful measure of PA. However, we expect that with a warmer climate, the difference between  $a_{tr}$  and  $a_r$  may diminish because an increasingly higher portion of  $T'_{NPA}(t)$  and  $T'_{NH}(t)$  variance will be yielded by trends.

The steadiness of model-based  $a_r$  (Fig. 7d) suggests that the relationship between NH and NPA SATs is preserved regardless of whether the preindustrial period or the last decades of the strongest anthropogenic warming are considered. Polar amplification may be described as an intrinsic mode of climate variability (Alexeev et al. 2005; Langen and Alexeev 2007); therefore, human-induced climate change will be projected on this mode without altering its spatial structure, in agreement with the concept of nonlinear climate dynamics perspective proposed by Palmer (1999). In that case, climate change and its variations at various time scales will produce similar estimates of PA.

Large-scale PA derived from observational data is evident from Table 2 with annual 1875–2008  $a_r = 1.62 \pm 0.10$ , close to the 1.56 estimated from ensemble-average PA derived from a suite of 42 CMIP model runs. There is a seasonal cycle with maximum PA in autumn and

spring (Table 2, Fig. 5). The former can be explained by local ice-albedo feedback mechanisms; however the latter cannot. Indeed, this seasonal cycle of PA is consistent with a large-scale winter and springtime “radiative” mechanism of PA and a year-round “advective” mechanism of PA, which is strongest in the cold season. The snow-albedo feedback mechanism may also be a plausible explanation for the springtime PA. During the last 15–20 years, PA during the cold season was very strong (Figs. 3 and 8). For example, in 2006–08 high-latitude winter–spring SATs were exceptionally high (Fig. 4). Unfortunately, observational SAT data preclude us from separating the contribution of “advective” and “radiative” mechanisms into the large-scale PA.

To ensure that our estimates of large-scale PA are not “contaminated” by effects of local ice-albedo feedbacks, we repeated our calculations of  $a_r$  presented in Table 2 by using NPA records from meteorological stations located at least 250 km away from the coast (Table 3). In general, the differences between these two calculations are small, within 15%. However, there is a substantial, almost twofold, increase of PA during the cold season. That may be a manifestation of a positive feedback mechanism among the SAT, available precipitable water, and incoming longwave radiation, which is strongest in regions with the lowest SATs. The inland meteorological stations have the lowest winter and spring SATs. Since

TABLE 2. Polar amplification (PA) calculated using the ratio of NPA and NH trends  $a_{tr}$  and the new measure  $a_r$  of PA, which links high-latitude and hemispheric temperature anomalies via regression relationship. For  $a_r$ , estimates shown as mean/SD.

	Annual		Winter		Spring		Summer		Autumn	
	$a_r$	$a_{tr}$								
1875–2008	1.62/0.10	1.72	1.23/0.14	1.73	1.54/0.13	1.74	1.27/0.08	1.63	1.59/0.12	1.48
1901–2008	1.45/0.11	1.30	1.10/0.16	1.42	1.44/0.14	1.44	1.20/0.08	1.17	1.49/0.15	0.99
1959–2008	1.52/0.14	1.56	1.14/0.22	1.44	1.68/0.21	1.86	1.21/0.11	1.13	1.58/0.20	1.77

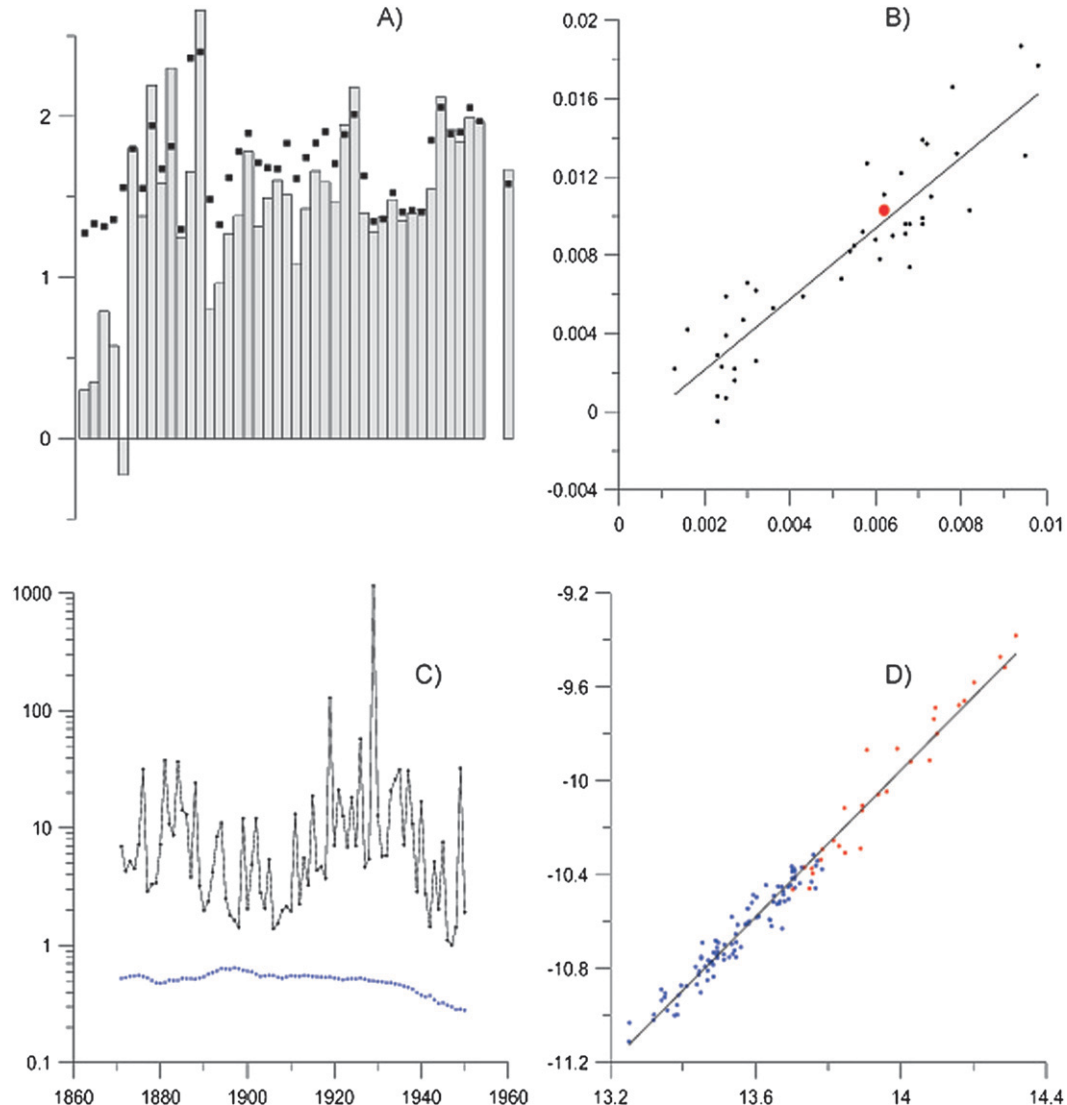


FIG. 7. Polar amplification from 42 CMIP models. (a)  $a_{tr}$  (bars) and  $a_r$  (black squares) for 1871–1999. For comparison the rightmost bar and black square show observation-based estimates. (b) Relationship between simulated trends for NH (horizontal axis) vs NPA (vertical axis) SATs. Red dot shows observation-based estimate;  $a_{tr}$  derived from this relationship is  $1.81 \pm 0.07$ . (c) Standard deviations of the ensemble-averaged indices  $a_{tr}$  (black) and  $a_r$  (blue) for a 50-yr running window. (d) Relationship between simulated ensemble-averaged NPA SATs (vertical axis) and NH SATs (horizontal axis). Linear regression is  $SAT_{NPA} = 1.56 \times SAT_{NH} - 31.83$ . Blue dots are for 1871–1970; red dots for 1971–99.

available precipitable water in the atmospheric column depends heavily on air temperature, and incoming longwave radiation is proportional to logarithm of precipitable water content (Zhang et al. 2001), the sensitivity of incoming longwave radiation to SAT change is higher for inland regions.

#### b. Local PA

PA at the local, Arctic-wide, scale is related to ice-albedo feedback mechanisms that are evident in maritime

areas in autumn when the ice cover is seasonally at a minimum (Figs. 4, 5, 9, and 10; e.g., Manabe and Stouffer 1994). For example, autumnal 1979–2008 SAT trends are amplified at the coastal stations in Siberia and the Canadian Archipelago (Fig. 5). SAT anomalies in autumns during recent years (2006–08) are strongest in the maritime NPA (Figs. 4 and 9). Strong linkage of ice-edge dynamics and air-sea heat fluxes (and SAT, not shown; e.g., Overland et al. 2008) is evident from Fig. 10. The SAT increase due to ice-albedo feedback may be traced

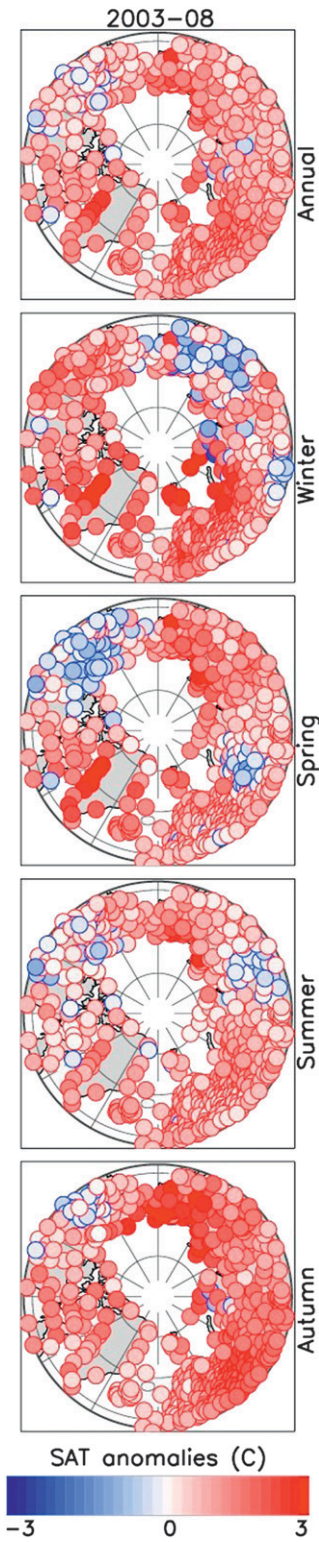


FIG. 8. SAT anomalies for 2003–08 relative to the mean defined over 1979–2008.

up to several hundred kilometers from the ice edge into the interior of the Siberian region, as evident from Fig. 9. Note also that, according to our dataset, the ice-albedo feedback mechanism is apparent during extended warm periods only (i.e., in the 1930s–40s and recent decades) and is not evident during cold periods (Fig. 9). However, we note that this may be partially due to a geometrical effect when the limited NPA used for our analysis does not include dynamics of the sea ice edge expanding far beyond the NPA.

Serreze et al. (2009), using NCEP reanalysis data, also found a dominant role of autumnal NPA warming in recent decades. However, our data suggest a relatively uniform spread of NPA warming over seasons in recent decades [cf. Fig. 3 from Serreze et al. (2009) and our Fig. 8]. Moreover, NPA SAT trends computed over extended time periods are stronger in winter and spring (Table 1). For example, over the last 50 years, the spring SAT trend was  $4.67^{\circ}\text{C}/100\text{ yr}$ , which is  $\sim 30\%$  stronger than the autumnal SAT trend. Only over the last three decades has the autumnal SAT trend exceeded slightly the winter and spring trends (Table 1). These results suggest that on the hemispheric scale the relative role of local ice-albedo feedback mechanisms may be moderate compared with the contribution of large-scale mechanisms of PA.

We further explore the role of ice-albedo feedback mechanisms in recent NPA warming over the Arctic Ocean. Oceanographic observations carried out in September 2007 showed a substantial—up to  $2^{\circ}\text{C}$  and more at some locations—water temperature increase in the upper  $h = 25\text{ m}$  layer in the Siberian sector of the Arctic Ocean, which has never been ice-free in the history of observations [Fig. 11; for data description, see Polyakov et al. (2009), manuscript submitted to *J. Phys. Oceanogr.*]. This upper ocean warming is used to estimate effects of atmospheric forcing due to a change of surface radiative properties. Based on these oceanographic observations, we estimate that the observed upper-ocean warming in summer 2007 led to an additional accumulation of heat of

$$Q = \oint dS \int_0^h \rho_w c_p (\Theta - \Theta_f) dz = 6.9 \times 10^{20} \text{ J},$$

where  $\Theta$  is potential temperature,  $\Theta_f$  is the freezing temperature at 0 db,  $\rho_w \approx 1030 \text{ kg m}^{-3}$  is water density, and  $c_p = 4186 \text{ J/(kg K)}$  is the specific heat of water in the area  $S \approx 2.4 \times 10^6 \text{ km}^2$  covered by the observations. Dynamical mechanisms such as wind-driven ice compression toward the western Arctic, enhanced transport of ice with the Transpolar Drift through Fram Strait, and ice export to Baffin Bay were the major cause for the dramatic summer 2007 ice loss (e.g., Nghiem et al. 2007). Therefore the portion of heat uptake used to melt ice in the summer 2007 opening is neglected in this analysis.

TABLE 3. Polar amplification defined by  $a_r$ , calculated using NPA records from meteorological stations located at least 250 km away from the coast and relative difference ( $D$ , %) of these estimates with those derived from all NPA records (Table 2).

	Annual		Winter		Spring		Summer		Autumn	
	$a_r$	$D$								
1875–2008	1.78	10	1.75	47	2.39	28	1.30	2	0.99	1
1901–2008	1.65	14	1.61	56	2.23	30	1.28	7	0.85	9
1959–2008	1.60	5	1.90	70	2.04	6	1.11	7	1.11	8

Note also that an increase of the upper-layer thickness in our calculation of  $Q$  led to a negligible increase in computed atmospheric heat uptake by the upper ocean. Normalized by  $S$ , this  $Q$  is equivalent to  $\sim 283 \text{ MJ m}^{-2}$  of heat content  $\tilde{Q}$ . This is  $\sim 65\%$  of the solar heating of  $440 \text{ MJ m}^{-2}$  estimated by Steele et al. (2008) based on satellite surface temperature observations in 2007, which covered the entire ice-free area of the Arctic Ocean. This apparent difference of estimates of  $\tilde{Q}$  may be partially due to the fact that satellites measure surface skin temperature, which in summer is higher than the temperature of the bulk of the upper ocean layer. One more potential reason for this difference is a limited area of oceanographic surveys compared with broader satellite-based coverage.

We compared the anomalous upper-ocean heat uptake caused by a change of surface albedo with the advective annual horizontal atmospheric heat transport through  $60^\circ\text{N}$ , which is estimated to be  $\sim 9.5 \times 10^{22} \text{ J}$ , with variations defined by a standard deviation (SD) of  $\sim 1.9 \times 10^{21} \text{ J}$ . These estimates were derived from Fig. 4 in Trenberth and Caron (2001) by multiplying power expressed in watts by the length of the year expressed in seconds. This SD is almost three times more than the total

amount of heat accumulated in the ice-free area in summer 2007. Despite its relatively small magnitude, the atmospheric effect of oceanic warming caused by ice reduction may be important due to strong near-surface atmospheric stratification leading to a large increase of atmospheric temperature near the surface (Deser et al. 2010). We note, however, that the autumnal PA can be traced over a limited ( $<500 \text{ km}$ ) area with a fast decay of SAT anomalies from the area of maximum ice retreat (Fig. 9), in good agreement with Ogi and Wallace (2007). Thus, we conclude that the recent dramatic reduction of arctic ice as well as anomalously high NPA SATs cannot be explained by the ice-albedo feedback mechanism alone. This conclusion agrees well with Graversen and Wang's (2009) findings. Using modeling experiments, Graversen and Wang showed that the ice-albedo feedback mechanism is responsible for only 15% of PA and that the impacts of water vapor and cloudiness dominate the PA of global warming.

## 5. Discussion

This study uses an extensive dataset of monthly SAT records from meteorological land stations. Most records have been updated by very recent (until December 2008) observations. The dataset includes previously unutilized sources, mostly from European Russia. The use of historical Russian archives provided spatiotemporal data coverage for this region of the NPA comparable to that for the Scandinavian region. Using this dataset, we document a large-scale year-round NPA warming rate of  $1.36^\circ\text{C century}^{-1}$  for 1875–2008, almost two times stronger than the NH trend ( $0.79^\circ\text{C century}^{-1}$ ). The rate of warming increased strongly in recent decades with exceptionally high SATs reaching  $1.72^\circ\text{C}$  in 2003,  $2.11^\circ\text{C}$

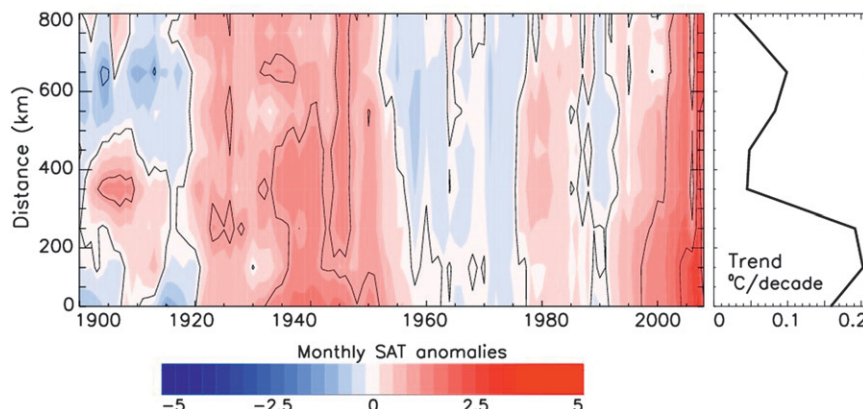


FIG. 9. (left) Plot of arctic autumnal SAT anomalies: year (x axis) vs distance from the coast (y axis, with zero at the coast and generally southward increase of distance from the Arctic Ocean). Polar amplification is evident during extended warm periods in the 1930–40s and recent decade. (right) Long-term (1900–2008) trend as a function of distance from the coast.

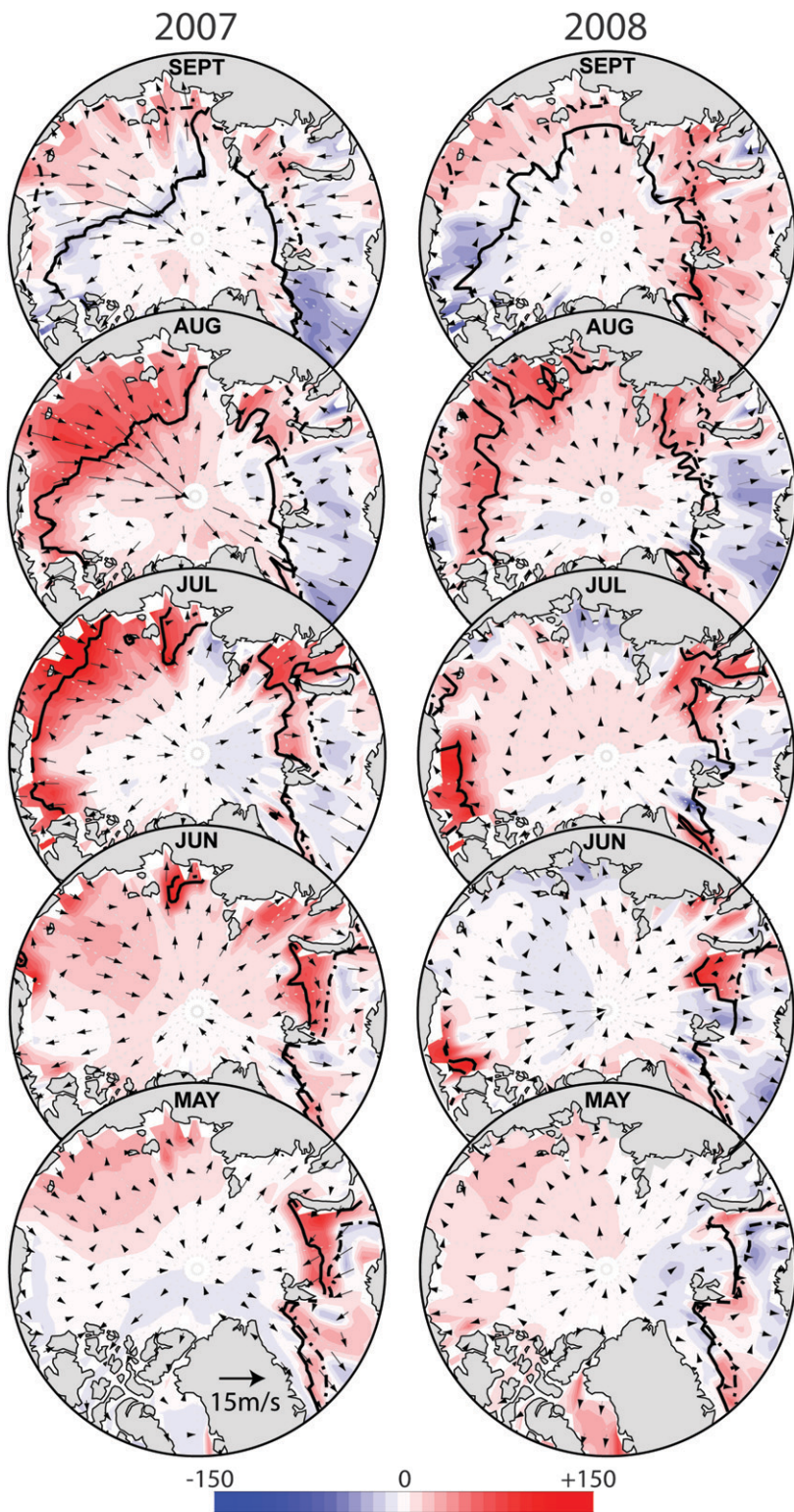


FIG. 10. Monthly mean atmospheric circulation (vectors) and anomalous net atmospheric heat fluxes (color,  $\text{W m}^{-2}$ ) in summer 2007 and 2008. Solid lines show monthly mean positions of ice edge; dashed-dotted lines show climatologic mean ice position. The NCEP reanalysis dataset is used for this figure.

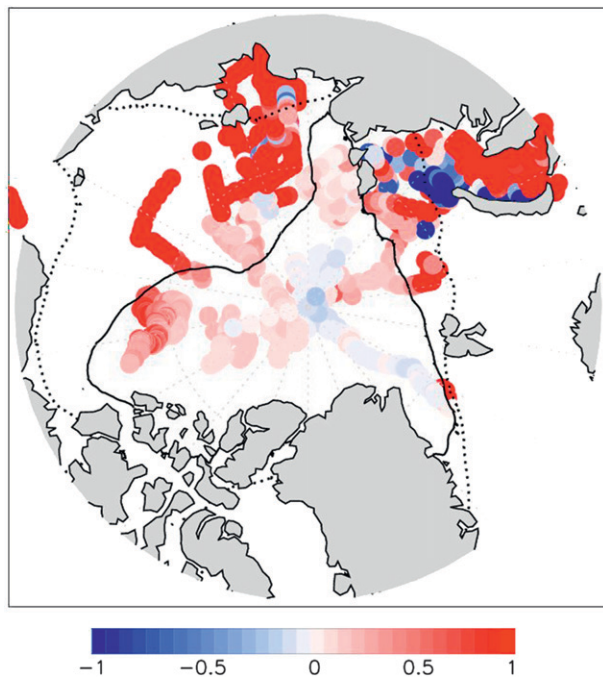


FIG. 11. Upper 25-m water temperature anomalies observed in summer 2007 [ $^{\circ}\text{C}$ , relative to climatology from Polyakov and Timokhov (1994), updated]. Solid lines show mid-September 2007 ice-edge position and dotted lines show climatologic mid-September ice-edge position.

in 2005, and  $2.18^{\circ}\text{C}$  in 2007, the warmest years in the history of instrumental observations.

Stronger warming in high-latitude regions, particularly in autumn and spring, is a manifestation of PA. The pattern of long-term SAT changes suggests two different spatial scales of mechanisms of PA: large-scale (hemispheric) and local (limited by NPA). Large-scale PA may be linked to both year-round hemispheric-in-scale atmospheric heat transports, which change the composition and vertical structure of the arctic atmosphere, and winter and springtime longwave radiative forcing linked to clouds and water vapor content. A combined effect of large-scale PA is evaluated using the new quantitative measure of PA  $a_r$ , linking NPA and NH temperature anomalies via a linear regression equation. For 1875–2008 this measure yields PA of  $1.62 \pm 0.10$ . This estimate of large-scale PA of global warming is very similar to the ensemble-average estimate of PA of 1.56 derived from a suite of 42 CMIP model runs (see caption for Fig. 7d).

Polar amplification at the local scale is related to ice-albedo feedback mechanisms, which are evident in autumn in maritime/coastal areas up to several hundred kilometers from the ice edge into the interior of continents. These mechanisms are apparent during extended warm periods only (i.e., in the 1930s–40s and recent decades) and are not evident during cold periods. Heat

budget estimates used to elaborate the role of ice-albedo feedback mechanisms suggest that the recent dramatic reduction of arctic ice as well as anomalously high NPA SATs cannot be explained by these mechanisms alone. We note, however, that further diminishing arctic summer ice cover will probably enhance the role of these mechanisms in shaping high-latitude climate change, consistent with the modeling results by Deser et al. (2010). Using modeling experiments, Deser et al. showed that the projected reduction of ice cover may result in increased heat transfer during winter and fall from the relatively warm ocean to the cold atmosphere, leading to a large increase of atmospheric temperature near the surface.

The attribution of PA of global warming to particular feedback mechanisms is a nontrivial task owing to gaps in observational data, short instrumental records, and strong high-latitude variability, particularly multidecadal variability. An important caveat is the poorly defined character of these mechanisms. For example, PA caused by natural variability and forced change may be different due to nonuniform geographical distribution of anthropogenic aerosol forcing. Anthropogenic climate change may be amplified or masked by natural variations, and these modes of variability can be separated only when the mechanisms governing them are better understood. There are substantial differences among estimates of radiative feedbacks associated with water vapor, lapse rate, clouds, and sea ice derived from general circulation models (Bony et al. 2006). Stephens (2005) provided a critical overview of the effects of clouds on the radiation budget of the global climate system. Stephens suggested that one of the key problems of present-day models lies in the imbedded cloud parameterizations and argued that “in view of the complex nature of the climate system, and the cumbersome problems encountered in diagnosing feedbacks, understanding cloud feedback will be gleaned neither from observations nor proved from simple theoretical argument alone. The blueprint for progress must follow a more arduous path that requires a carefully orchestrated and systematic combination of model and observations” (p. 269). Therefore, advances in modeling and theory as well as continued observations are required in order to develop a deeper understanding of the nature of PA of global warming, which is a necessary step for developing a predictive system of future climate change.

## 6. Conclusions

In summary, we formulate the major results of this study:

- Using a new extensive dataset of Arctic SATs, including previously unutilized historical Russian data,

we documented a high-latitude warming rate of  $1.36^{\circ}\text{C century}^{-1}$  for 1875–2008, with an exceptionally strong warming rate in the recent decade ( $1.35^{\circ}\text{C decade}^{-1}$ ).

- A new stable statistical measure of polar amplification (PA) linking high-latitude and hemispheric annual temperature anomalies via a regression relationship is proposed. For 1875–2008, this measure yields PA of  $\sim 1.62$ .
- Local PA related to the ice–albedo feedback mechanisms is autumnal and coastal, extending several hundred kilometers inland. A recent reduction of Arctic Ocean sea ice and anomalously high SATs cannot be explained by the ice–albedo feedback mechanisms alone, and the role of large-scale mechanisms of PA of global warming may be important.

**Acknowledgments.** This study was supported by JAMSTEC (RB, IP, VA), NSF (IP, VA), NASA (IP), and Russian Foundation for Basic Research (RB, Grant RFBR 08-05-00569-a) grants. We thank D. Atkinson, P. Jones, P. Groisman, and M. Shulski for data; U. Bhatt, R. Graversen, and J. Walsh for useful comments; T. Pavlova for climate models time series; and J. Moss for help with the graphics. We acknowledge the modeling

groups, the Program for Climate Model Diagnosis and Intercomparison (PCMDI) and the WCRP’s Working Group on Coupled Modelling (WGCM) for their roles in making available the WCRP CMIP3 multi-model dataset. Support of this dataset is provided by the Office of Science, U.S. Department of Energy.

## APPENDIX A

### Statistical Procedure of Data Quality Control

Available hourly or daily data were averaged to obtain monthly values. Statistical control of data quality was based on two methods. The first one is based on statistical distribution of random variable  $\nu$ :

$$\nu = \frac{x - \bar{x}}{S(x)}, \quad (\text{A1})$$

which is a normalized anomaly of random variable  $x$  (in our case, hourly or daily SATs; see also Cramer 1999), where  $\bar{x}$  is the mean and  $S(x)$  is the square root deviation. The density distribution of random variable  $\nu$  may be described by the following relationship:

$$f(\nu) = \begin{cases} \frac{1}{\sqrt{\pi(n-1)}} \frac{\Gamma\left(\frac{n-1}{2}\right)}{\Gamma\left(\frac{n-2}{2}\right)} \left(1 - \frac{\nu^2}{n-1}\right)^{(n/2)-2}, & |\nu| < \sqrt{n-1} \\ 0, & |\nu| \geq \sqrt{n-1}, \end{cases} \quad (\text{A2})$$

where  $n$  is the number of observations and  $\Gamma$  is the gamma function. The following procedure of error estimate has been used. For each month, station data were used to calculate  $\bar{x}$  and  $S(x)$ . The random variable  $\nu$  is obtained by Eq. (A1) and each  $\nu$  is compared to the critical value  $\nu_{cr}$ , which is obtained by solving numerically the following equation:

$$0.5 + \int_0^{\nu_{cr}} f(\nu) d\nu = 1 - \alpha, \quad (\text{A3})$$

where  $\alpha$  is the level of statistical significance. Note that expression (A2) for density distribution was obtained based on an assumption of independence of samples. Therefore, this criterion does not always distinguish and remove errors from meteorological data, particularly because these data are subject to daily and annual cycles.

The second method uses Dixon’s criteria (Dixon 1983). This method is based on comparison and removal of extreme values from the available record and is less sensitive to autocorrelation and seasonality in the time

series. Station hourly or daily meteorological observations are subject to quality control for each month. First, two maximal  $x_{\max,1}$  and  $x_{\max,2}$  and two minimal  $x_{\min,1}$  and  $x_{\min,2}$  values ( $x_{\max,1} \geq x_{\max,2}$  and  $x_{\min,1} \leq x_{\min,2}$ ) are found in each monthly segment of the time series. Second, Dixon’s statistics are defined as

$$d_{\max} = \frac{x_{\max,1} - x_{\max,2}}{x_{\max,1} - x_{\min,1}}, \quad (\text{A4})$$

and

$$d_{\min} = \frac{x_{\min,2} - x_{\min,1}}{x_{\max,1} - x_{\min,1}}. \quad (\text{A5})$$

If random variables  $d_{\max}$  and  $d_{\min}$  exceed the tabulated critical value  $d_{cr}$ , then the corresponding  $x$  is considered as an erroneous value and removed from the record. The procedure is repeated until all remaining values satisfy Dixon’s criteria. Analysis of method performance showed that the values identified by Dixon’s method as erroneous

were, indeed, erroneous. Effects of urban warming are not considered in this study. It is known, however, that these effects are insignificant for long-term spatially averaged SAT (Jones et al. 1989; Parker 2004; Peterson and Vose 1997).

## APPENDIX B

### Procedure for Estimating the Statistical Significance of Trends Using a Nonparametric Approach

Let us consider a discrete sampling of a process  $Y(t)$  with  $N$  available values (i.e.,  $Y_i$ ,  $i = 1, N$ ). The linear dependence of  $Y(t)$  of time may be described by the following model:

$$Y(t) = a + bt + \varepsilon(t), \quad (\text{B1})$$

where the linear function  $a + bt$  approximates systematic change of the parameter  $Y(t)$  and the random term  $\varepsilon(t)$  describes natural internal variability of the system as well as random external forcing. Time  $t$  is defined over the interval  $[-T/2, T/2]$ . The coefficient  $a$  corresponds to the mean value of  $Y(t)$  and the coefficient  $b$  defines trend;  $a$  and  $b$  may be found by the following formulas:

$$a = \langle Y \rangle = N^{-1} \sum_{i=1}^N Y_i \quad (\text{B2})$$

and

$$b = \frac{\langle Y(t)t \rangle}{\langle t^2 \rangle} = \sum_{i=1}^N Y_i t_i / \sum_{i=1}^N t_i^2, \quad (\text{B3})$$

where the angle brackets correspond to time averaging.

Statistical significance of a linear trend may be estimated by an algorithm based on an estimation of variance of the sample trend and on introducing statistics with a distribution close to the Student's  $t$  distribution. We note that variance of both sample mean and sample linear trend is asymptotically defined by the spectral density at zero frequency (Bloomfield 1992; Bloomfield and Nychka 1992; Von Storch and Zwiers 1999):

$$D_b(T) = \frac{12 \times 2\pi S(0)}{T^3}, \quad (\text{B4})$$

where  $S(\omega)$  is the spectral density of a process at frequency  $\omega$  and the period  $T$  is defined by the time series length as  $T = (N - 1)\Delta t$  in which time step  $\Delta t$  is assumed to be equal to 1. Our proposed method of estimating statistical significance of trends is based on the use of statistics similar to Student's  $t$  statistics  $S_b = b/\sigma_b$ , where  $\sigma_b$  is estimated using sample spectral density at zero frequency. Similar statistics were used for estimates of

sample mean ( $S_{\bar{X}} = \bar{X}/\sigma_{\bar{X}}$ ) and the sample trend by Brillinger (1981), Zwiers and Thiebaux (1987), and Fomby and Vogelsang (2002). Estimates of sample mean and variance of sample mean based on spectral density  $S(0)$  are statistically independent (Zwiers and Thiebaux 1987). However, estimates of sample trend  $b$  and spectral density  $S(0)$  are not [ $b$  and  $S(0)$  are always correlated], which may lead to false conclusions. To resolve this problem, we propose to detrend the sample prior to statistical analysis. In this case, sample trend  $b$  and spectral density at zero frequency  $S(0)$  are practically always uncorrelated, which allows us to use statistics similar to Student's  $t$ . Detrending, however, distorts the sample spectrum, which is corrected in the algorithm using correction factors. One more effect of this procedure is reduction of effective degrees of freedom by one. The following are the proposed algorithm steps.

- 1) Compute the mean value  $\bar{Y} = N^{-1} \sum_{i=1}^N Y_i$  and reduce time series to anomalies  $Z_i = Y_i - \bar{Y}$ .
- 2) Compute sample trend (i.e., linear regression coefficient):

$$b = \sum_{i=1}^N Z_i [i - (N + 1)/2] / \sum_{i=1}^N [i - (N + 1)/2]^2. \quad (\text{B5})$$

- 3) Detrend the time series for anomalies  $Z_i$  by removing its linear component:

$$X_i = Z_i - b \left[ i - \frac{1}{2}(N + 1) \right]. \quad (\text{B6})$$

- 4) Estimate spectral density of the random function  $X(t)$  at zero frequency. According to recommendations from Jenkins and Watts (1968), the maximum number of lags  $M$  of the autocorrelation function for estimation of spectral density should be 0.1 of the time series length  $N$  (i.e.,  $M = N/10$ ). The effective degree of freedom  $N_{e,s}$  for spectral density at zero frequency is  $N_{e,s} = 5$ .
- 4a) Estimate values of sample variance and sample  $\sigma_x$  as

$$\sigma_x^2 = (N - 1)^{-1} \sum_{i=1}^N X_i^2, \quad \sigma_x = \sqrt{\sigma_x^2}, \quad (\text{B7})$$

- 4b) Normalize the time series by  $\sigma_x$ :

$$X'_i = X_i / \sigma_x. \quad (\text{B8})$$

- 4c) Estimate the correlation function of  $X'$  for shifts  $i = 1, M$ :

$$r(i) = (N - i)^{-1} \sum_{k=1}^{N-i} X'_k X'_{k+i}. \quad (\text{B9})$$

- 4d) Estimate normalized spectral density at zero frequency:

$$S_{X'}(0) = \frac{1}{\pi} \left( 0.5 + \sum_{i=1}^M r(i) \right). \quad (\text{B10})$$

If the spectral density is negative,  $S_{X'}(0) < 0$ , estimate  $S_{X'}(0)$  again using the Tukey weight function:

$$S_{X'}(0) = \frac{1}{\pi} \left\{ 0.5 + \sum_{i=1}^{M-1} r(i)[1 + \cos(\pi i/M)]/2 \right\}. \quad (\text{B11})$$

- 4e) Obtain spectral density by multiplying the estimate of normalized spectral density  $S_{X'}(0)$  by the estimate of variance  $\sigma_X^2$ :

$$S_X(0) = S_{X'}(0)\sigma_X^2. \quad (\text{B12})$$

- 4f) Correct  $S_X(0)$  in order to eliminate systematic errors of the estimate of the correlation function due to estimates of sample mean and detrending of time series:

$$S_Z(0) = S_X(0)\Delta, \quad (\text{B13})$$

where  $\Delta = N_{e,s}/(N_{e,s} - 2)$ .

- 5) Estimate the variance of the sample trend

$$D_b = \frac{24\pi}{(N-1)^3} S_Z(0). \quad (\text{B14})$$

- 6) Estimate the sample  $\sigma_b$

$$\sigma_b = \sqrt{D_b}. \quad (\text{B15})$$

- 7) Include statistics  $S_b = b/\sigma_b$ , which have a Student's  $t$  statistical distribution in the case of the normally distributed original time series.
- 8) Because of detrending of the original time series of anomalies  $Z(t)$ , the effective number of degrees of freedom for the statistics  $S_b$  is decreased by 1:  $N_{\text{eff}} = N_{e,s} - 1$ . Therefore, using the recommended  $M = 0.1N$ , which corresponds to  $N_{e,s} = 5$ , we have  $N_{\text{eff}} = 4$ .

- 9) Using critical values of the Student's distribution  $t_\alpha$ , formulate the decisive rule: in the case of  $|S_b| > t_\alpha$ , the null hypothesis (i.e., the hypothesis of the nonexistence of trend) is rejected with probability  $1 - \alpha$ .
- 10) In general cases, the Student's  $t$  distribution function is expressed via hypergeometric functions; however, for the number of degrees of freedom  $n = N_{\text{eff}} = 4$ , the probability of null hypothesis rejection may be easily described by the expression

$$\begin{aligned} F(S_b) &= 2 \int_0^{|S_b|} \frac{\Gamma\left(\frac{n+1}{2}\right)}{\sqrt{n\pi}\Gamma\left(\frac{n}{2}\right)} \left(1 + \frac{x^2}{n}\right)^{-(n+1)/2} dx \\ &= \frac{3}{4} \int_0^{|S_b|} \left(1 + \frac{x^2}{4}\right)^{-5/2} dx = \frac{|S_b|(6 + S_b^2)}{(4 + S_b^2)^{3/2}}. \end{aligned} \quad (\text{B16})$$

Thus, using computed statistics  $S_b$ , by (B16) we may obtain the probability of null hypothesis rejection.

The proposed algorithm for estimating statistical significance of linear trends is based on an estimate of sample spectral density at zero frequency of the preliminary detrended time series. This approach leads to a noncorrelated sample trend and its variance and allows statistics similar to Student's  $t$ .

## REFERENCES

- ACIA, 2005: *Arctic Climate Impact Assessment*. Cambridge University Press, 1042 pp.
- Alexeev, V. A., 2003: Sensitivity to CO<sub>2</sub> doubling of an atmospheric GCM coupled to an oceanic mixed layer: A linear analysis. *Climate Dyn.*, **20**, 775–787.
- , P. L. Langen, and J. R. Bates, 2005: Polar amplification of surface warming on an aquaplanet in “ghost forcing” experiments without sea ice feedbacks. *Climate Dyn.*, **24**, 655–666, doi:10.1007/s00382-005-0018-3.
- Belchansky, G. I., D. C. Douglas, and N. G. Platonov, 2008: Fluctuating Arctic sea ice thickness changes estimated by an in situ learned and empirically forced neural network model. *J. Climate*, **21**, 716–729.
- Bloomfield, P., 1992: Trends in global temperature. *Climatic Change*, **21**, 1–16.
- , and D. Nychka, 1992: Climate spectra and detecting climate change. *Climatic Change*, **21**, 275–287.
- Bony, S., and Coauthors, 2006: How well do we understand and evaluate climate change feedback processes? *J. Climate*, **19**, 3445–3482.
- Brillinger, D. R., 1981: *Time Series: Data Analysis and Theory*. Holden Day, 540 pp.
- Brohan, P., J. J. Kennedy, I. Harris, S. F. B. Tett, and P. D. Jones, 2006: Uncertainty estimates in regional and global observed temperature changes: A new data set from 1850. *J. Geophys. Res.*, **111**, D12106, doi:10.1029/2005JD006548.

- Climatologic Reference Book of the USSR, 1954a: *Karelo-Finskaya SSR: Meteorological Data for Selected Years*. Vol. 2, Part I: Air Temperature, Hydrometeoizdat, 185 pp.
- , 1954b: *Leningrad, Pskov, and Novgorod Regions: Meteorological Data for Selected Years*. Vol. 3, Part I: Air Temperature, Hydrometeoizdat, 346 pp.
- , 1954c: *Estonia SSR: Meteorological Data for Selected Years*. Vol. 4, Part I: Air Temperature, Hydrometeoizdat, 608 pp.
- , 1954d: *Molotov, Sverdlovsk, Cheliabinsk, Kurgan Regions, and Bashkir ASSR: Meteorological Data for Selected Years*. Vol. 9a, Part I: Air Temperature. Hydrometeoizdat, 513 pp.
- , 1956: *Murmansk and Archangel Regions and Komi ASSR: Meteorological Data for Selected Years*. Vol. 1, Part I: Air Temperature, Hydrometeoizdat, 563 pp.
- , 1957: *Krasnoyarsky Krai: Meteorological Data for Selected Years*. Vol. 21, Part I: Air Temperature, Hydrometeoizdat, 217 pp.
- , 1962: *Vologodsky Region: Meteorological Data for Selected Years*. Vol. I, Parts I–VIII: Air Temperature, Precipitation, Snow Cover, Wind, Humidity, Cloudiness, Sunshine, Soil Temperature, Fogs, Thunderstorms, Blizzards, Air Pressure, Hail, Hydrometeoizdat, 600 pp.
- Comiso, J. C., C. L. Parkinson, R. Gersten, and L. Stock, 2008: Accelerated decline in the Arctic sea ice cover. *Geophys. Res. Lett.*, **35**, L01703, doi:10.1029/2007GL031972.
- Cramer, H., 1999: *Mathematical Methods of Statistics*. 19th ed. Princeton University Press, 575 pp.
- Dery, S. J., and R. D. Brown, 2007: Recent Northern Hemisphere snow cover extent trends and implications for the snow-albedo feedback. *Geophys. Res. Lett.*, **34**, L22504, doi:10.1029/2007GL031474.
- Deser, C., R. Tomas, M. Alexander, and D. Lawrence, 2010: The seasonal atmospheric response to projected Arctic sea ice loss in the late twenty-first century. *J. Climate*, **23**, 333–351.
- Dixon, W. J., 1983: *Introduction to Statistical Analysis*. 4th ed. McGraw-Hill, 672 pp.
- Fetterer, F., and V. Radionov, 2000: The Environmental Working Group arctic meteorology and climate atlas. National Snow and Ice Data Center. [Available online at [http://nsidc.org/data/docs/noaa/g01938\\_ewg\\_arctic\\_met\\_atlas/](http://nsidc.org/data/docs/noaa/g01938_ewg_arctic_met_atlas/).]
- Fomby, T. B., and T. J. Vogelsang, 2002: The application of size-robust trend statistics to global warming temperature series. *J. Climate*, **15**, 117–123.
- Francis, J. A., and E. Hunter, 2007: Changes in the fabric of the Arctic's greenhouse blanket. *Environ. Res. Lett.*, **2**, 045011, doi:10.1088/1748-9326/2/4/045011.
- Graversen, R. G., and M. Wang, 2009: Polar amplification in a coupled climate model with locked albedo. *Climate Dyn.*, **33**, 629–643, doi:10.1007/s00382-009-0535-6.
- Holland, M. M., and C. M. Bitz, 2003: Polar amplification of climate change in coupled models. *Climate Dyn.*, **21**, 221–232.
- Jenkins, G. M., and D. G. Watts, 1968: *Spectral Analysis and Its Applications*. Holden-Day, 525 pp.
- Jones, P. D., and A. Moberg, 2003: Hemispheric and large-scale surface air temperature variations: An extensive revision and an update to 2001. *J. Climate*, **16**, 206–223.
- , P. M. Kelly, C. M. Goodess, and T. Karl, 1989: The effect of urban warming on the Northern Hemisphere temperature average. *J. Climate*, **2**, 285–290.
- , M. New, D. E. Parker, S. Martin, and I. G. Rigor, 1999: Surface air temperature and its changes over the past 150 years. *Rev. Geophys.*, **37**, 173–199.
- Kalnay, E., and Coauthors, 1996: The NCEP/NCAR 40-Year Reanalysis Project. *Bull. Amer. Meteor. Soc.*, **77**, 437–471.
- Langen, P. L., and V. A. Alexeev, 2005: Analysis of  $2 \times \text{CO}_2$  sensitivity in an aquaplanet GCM using the fluctuation–dissipation theorem. *Geophys. Res. Lett.*, **32**, L23708, doi:10.1029/2005GL024136.
- , and —, 2007: Polar amplification as a preferred response in an aquaplanet GCM. *Climate Dyn.*, **29**, 305–317, doi:10.1007/s00382-006-0221-x.
- Lindsay, R. W., and J. Zhang, 2005: The thinning of Arctic sea ice, 1988–2003: Have we passed a tipping point? *J. Climate*, **18**, 4879–4894.
- , —, A. J. Schweiger, M. A. Steele, and H. Stern, 2009: Arctic sea ice retreat in 2007 follows thinning trend. *J. Climate*, **22**, 165–176.
- Manabe, S., and R. J. Stouffer, 1980: Sensitivity of a global climate model to an increase of  $\text{CO}_2$  concentration in the atmosphere. *J. Geophys. Res.*, **85**, 5529–5554.
- , and —, 1994: Multiple-century response of a coupled ocean–atmosphere model to an increase of atmospheric carbon dioxide. *J. Climate*, **7**, 5–23.
- Meehl, G. A., C. Covey, T. Delworth, M. Latif, B. McAvaney, J. F. B. Mitchell, R. J. Stouffer, and K. E. Taylor, 2007: The WCRP CMIP3 multimodel dataset: A new era in climate change research. *Bull. Amer. Meteor. Soc.*, **88**, 1383–1394.
- Meier, W. N., J. Stroeve, and F. Fetterer, 2007: Whither Arctic sea ice? A clear signal of decline regionally, seasonally, and extending beyond the satellite record. *Ann. Glaciol.*, **46**, 428–434.
- Murray, C., and J. Walsh, 2005: A model ensemble assessment of the environment of arctic warming by sea ice retreat. *SOLA*, **1**, 57–60.
- Nghiem, S. V., I. G. Rigor, D. K. Perovich, P. Clemente-Colón, J. W. Weatherly, and G. Neumann, 2007: Rapid reduction of Arctic perennial sea ice. *Geophys. Res. Lett.*, **34**, L19504, doi:10.1029/2007GL031138.
- Ogi, M., and J. M. Wallace, 2007: Summer minimum Arctic sea ice extent and the associated summer atmospheric circulation. *Geophys. Res. Lett.*, **34**, L12705, doi:10.1029/2007GL029897.
- Overland, J. E., M. Wang, and S. Salo, 2008: The recent Arctic warm period. *Tellus*, **60A**, 589–597.
- Palmer, T. N., 1999: A nonlinear dynamical perspective on climate prediction. *J. Climate*, **12**, 575–591.
- Parker, D. E., 2004: Large-scale warming is not urban. *Nature*, **432**, 290.
- Peterson, T. C., and R. S. Vose, 1997: An overview of the Global Historical Climatology Network temperature database. *Bull. Amer. Meteor. Soc.*, **78**, 2837–2849.
- Polyakov, I. V., and L. A. Timokhov, 1994: Mean fields of temperature and salinity of the Arctic Ocean. *Russ. Meteor. Hydrol.*, **7**, 33–38.
- , and M. A. Johnson, 2000: Arctic decadal and interdecadal variability. *Geophys. Res. Lett.*, **27**, 4097–4100.
- , and Coauthors, 2002: Observationally based assessment of polar amplification of global warming. *Geophys. Res. Lett.*, **29**, 1878, doi:10.1029/2001GL011111.
- , and Coauthors, 2005: One more step toward a warmer Arctic. *Geophys. Res. Lett.*, **32**, L17605, doi:10.1029/2005GL023740.
- , and Coauthors, 2008: Arctic Ocean freshwater changes over the past 100 years and their causes. *J. Climate*, **21**, 364–384.

- Rind, D., R. Healy, C. Parkinson, and D. Martinson, 1995: The role of sea ice in  $2 \times \text{CO}_2$  climate model sensitivity. Part I: The total influence of sea ice thickness and extent. *J. Climate*, **8**, 449–463.
- Rubinshteyn, E., Ed., 1930: *Monthly Air Temperature for the Eurasian part of the USSR for Selected Years, Northward from 55°N*. Vol. 2, *Air Temperature, Climate of the USSR: Part I*, MGO Publications, 180 pp.
- , 1933: *Monthly Air Temperature for the Asian Part of the USSR for Selected Years*. Vol. 4, *Air Temperature, Climate of the USSR: Part I*, MGO Publications, 258 pp.
- Schneider, E. K., R. S. Lindzen, and B. P. Kirtman, 1997: A tropical influence on global climate. *J. Atmos. Sci.*, **54**, 1349–1358.
- , B. P. Kirtman, and R. S. Lindzen, 1999: Tropospheric water vapor and climate sensitivity. *J. Atmos. Sci.*, **56**, 1649–1658.
- Serreze, M. C., and J. A. Francis, 2006: The arctic amplification debate. *Climatic Change*, **76**, 241–264.
- , A. P. Barrett, J. C. Stroeve, D. N. Knidig, and M. M. Holland, 2009: The emergence of surface-based Arctic amplification. *Cryosphere*, **3**, 11–19.
- Steele, M., W. Ermold, and J. Zhang, 2008: Arctic Ocean surface warming trends over the past 100 years. *Geophys. Res. Lett.*, **35**, L02614, doi:10.1029/2007GL031651.
- Stephens, G. L., 2005: Cloud feedbacks in the climate system: A critical review. *J. Climate*, **18**, 237–273.
- Stroeve, J., and Coauthors, 2008: Arctic sea ice extent plummets in 2007. *Eos, Trans. Amer. Geophys. Union*, **89**, 13–20, doi:10.1029/2008EO020001.
- Trenberth, K. E., and J. M. Caron, 2001: Estimates of meridional atmosphere and ocean heat transport. *J. Climate*, **14**, 3433–3443.
- Vinnikov, K. Ya., G. V. Gruza, V. F. Zakharov, A. A. Kirillov, N. P. Kovyneva, and E. Ya. Rankova, 1980: Recent climatic changes in the Northern Hemisphere. *Soviet Meteor. Hydrol.*, **6**, 1–10.
- Von Storch, H., and F. W. Zwiers, 1999: *Statistical Analysis in Climate Research*. Cambridge University Press, 494 pp.
- Walsh, J. E., and W. L. Chapman, 2001: 20th-century sea-ice variations from observational data. *Ann. Glaciol.*, **33**, 444–448.
- Winton, M., 2006: Amplified Arctic climate change: What does surface albedo feedback have to do with it? *Geophys. Res. Lett.*, **33**, L03701, doi:10.1029/2005GL025244.
- Zhang, T., K. Stamnes, and S. A. Bowling, 2001: Impact of atmospheric thickness on the atmospheric downwelling longwave radiation and snowmelt under clear-sky conditions in the arctic and subarctic. *J. Climate*, **14**, 920–939.
- Zwiers, F. W., and H. J. Thiebaux, 1987: Statistical considerations for climate experiments. Part I: Scalar tests. *J. Climate Appl. Meteor.*, **26**, 464–476.